High-amplitude oscillatory events orchestrate cortical activity for efficient cognition

Marcus Siems[1]*, Yinan Cao[1], Tobias H. Donner[1], Konstantinos Tsetsos[1,2+], & Andreas K. Engel[1+]

[1] Department of Neurophysiology and Pathophysiology, University Medical Center Hamburg-Eppendorf, Hamburg, Germany

[2] School of Psychological Science, University of Bristol, Bristol, United Kingdom

* Corresponding author

[+] Contributed equally

Contact Information

Correspondence: m.siems@uke.de

Summary

How do large-scale functional brain networks dynamically emerge to enable cognition? Correlated oscillations, a mechanism for inter-areal interactions, can be expressed as phase coherence or correlated amplitude fluctuations. However, little is known about whether and how the amplitude correlation of cortical oscillations can impact cognition. Here, we demonstrate that inter-areal amplitude coupling related to cognitive dynamics mainly reflects transient coincidences of high-amplitude oscillatory events, rather than sustained coupling of oscillations. Capitalizing on the spatio-temporal resolution of brain-wide magnetoencephalography (MEG) during a task probing attention and decision-making our findings reveal behaviorally relevant transient networks: First, coincidence of high-amplitude oscillatory events in the alpha and beta frequency range increases prior to correct decisions in a parieto-frontal network. Second, during attention allocation coincident high-amplitude events increase in visual, medial parietal and lateral prefrontal networks in the theta/alpha frequency range. We propose that the brain-wide orchestration of high-amplitude oscillatory events can facilitate inter-areal interactions supporting efficient cognition.

Introduction

Cognition requires the exchange of information represented in distant areas of the brain. A central question in neuroscience is, thus, how local activity can be orchestrated between distant brain areas to integrate information needed for cognitive processes and goal-directed actions. A growing body of literature proposes neural oscillations, reflecting excitability fluctuations in local neuronal assemblies, as a temporal feature improving this information exchange[1–5]. Correlations between local oscillations have been proposed to facilitate the flexible reconfiguration of brain networks to meet the cognitive and behavioral demands posed by a dynamic environment[1,6–10]. Considerable work has investigated the functional role of coherence of the phase of neural oscillations for inter-areal communication[8,11]. Yet, a second mode of intrinsic inter-areal coupling has been described which relies on the coupling of the amplitude of local population activity[6,7,12–14]. How amplitude coupling can aid dynamic inter-areal communication for adaptive behavior has, however, remained elusive. We here propose that temporally precise interactions between distant brain areas can be enabled through the coincidence of high-amplitude oscillatory events and we present an empirical test of this hypothesis.

So far, there is a considerable gap in the current understanding of the two brain-wide intrinsic coupling modes[6,7]. A growing body of literature demonstrates that phase coupling, physiologically constrained through conduction delays, might enable or disable communication by aligning local excitability fluctuations and (oscillatory) spiking input with millisecond precision[3,8,9,11] and modulate in a task-specific manner during cognition[11,15–20] and perception[21–23]. In contrast, the mechanisms underlying neuronal information channels mirrored in amplitude coupling are not well understood. What has been shown in recent years is that time-averaged amplitude coupling is linked to perception[22], memory[24], and decision-making[25] and can dissociate from phase coupling in task[26,27], rest[12] and disease[28]. A major unresolved question is whether,

and how, the coupling of local signal amplitudes could enable temporally precise interactions between distant brain areas necessary for adaptive behavior.

Recent studies resolving coupling modes dynamically over time[29] can help to elucidate the role of amplitude co-fluctuations in cognition. A growing body of evidence shows that transient high-amplitude events locally interfuse sustained bandlimited neuronal activity[3,20,30–35]. Importantly, not every event is the same and high-amplitude events can originate from both, oscillatory or aperiodic transients[3,34,36]. High-amplitude oscillatory events[30,37,38] reflect rhythmic excitability fluctuations, can result from synchronization in neuronal populations without firing rate modulation and display narrow-band spectral power increases[4,20,39]. On the other hand, aperiodic activity, another meaningful feature of healthy brain function, which is modulated during cognition[39–41] and linked to time varying firing rate fluctuations[3,42], can display transient increases as well[36,37,39]. We, thus, conjecture that transiently high-amplitude oscillatory and aperiodic events as well as sustained low-amplitude activity might provide potentially distinct information channels for neuronal interactions[3,42–44]. If this assumption holds true, dissecting sustained amplitude coupling from transient oscillatory and aperiodic events should reveal distinct functional networks with dissociable relations to behavior.

Here, we hypothesize that coincident high-amplitude oscillatory and aperiodic events[3,42] enable the rapid reconfiguration of cortical networks required for flexible behavior. To test this hypothesis, we leverage spatio-temporally precise magnetoencephalography (MEG) recordings with whole-brain coverage to comprehensively unravel sustained and transient components of cortical activity during a challenging cognitive task[45]. Specifically, we utilize transient high-amplitude events coinciding in distant areas to define functional networks and contrast our findings to sustained amplitude co-fluctuations. Assessing time-resolved signal rhythmicity[29,37] enables us to separate oscillatory and aperiodic high-amplitude event subtypes.

We find that predominantly coincident high-amplitude oscillatory events, but not sustained network activity, display behavioral relevance for decision-making and are modulated during

attention allocation. Moreover, brain-wide networks defined by the coincidence of high-amplitude oscillatory events replicate previously observed functional networks defined by averaged amplitude co-fluctuations[12,13]. Overall, our findings demonstrate that for efficient cognition and behavior cortical network activity can be shaped and dynamically regulated through transiently occurring high-amplitude events. We, thus, propose that the temporally precise orchestration of high-amplitude oscillatory events coinciding in distant brain areas is a key signature of large-scale cortical interactions that can enable efficient cognition.

Results

Large-scale neuronal activity can be considered as a vast space-time landscape of intensity fluctuations (Fig. 1). We argue that transiently occurring high-amplitude oscillatory events play a unique role in large-scale interactions. To this end, the orchestration of high-amplitude events needs to be temporally precise, i.e., coincidental, between distant brain areas to form dynamic and flexible networks (Fig. 1a). We further assume that the temporal coincidence of high-amplitude events between areas processing relevant information at critical time points, e.g., during stimulus onset, can impact behavior (Fig. 1b).

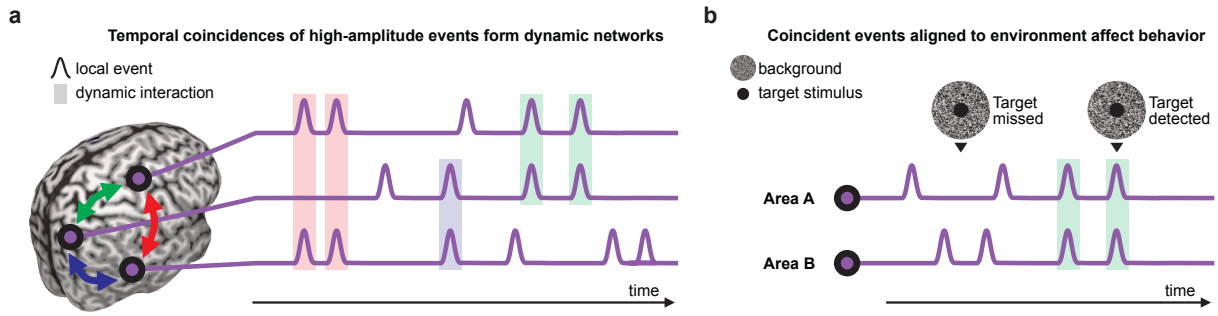

Figure 1 | Schematic of high-amplitude oscillatory events orchestrating cortical activity for efficient cognition. **a** Temporal formation of dynamic networks (colored arrows) defined through coincident high-amplitude events (colored shading). **b** Dynamic networks forming by coincidence of events during critical periods of a task, for example the onset of a target stimulus, might impact performance in an attention task.

We put this framework to the test and recorded magnetoencephalography (MEG) from twenty participants (9 female, age_{mean} = 28.05 years ± age_{STD} 4.6 years) to non-invasively assess high-amplitude events in the healthy human brain. During the recording the participants performed a challenging three-alternative decision-making task comparing the contrast of three Gabor patches ($median_{accuracy}$ = 77%, $range_{accuracy}$ = 66–86%) presented at different peripheral locations equidistant from fixation and with variable task framing (for details on the task see Methods and [45]).

We harnessed (oscillatory) events to directly establish functional coupling, reflected in temporal coincidence of high-amplitude activity in distant cortical sources. In the following, we will refer to functional coupling based on high-amplitude oscillatory event coincidences as OECs. We here applied the analyses of event coincidences and of amplitude coupling to pairwise orthogonalized signals to discount spurious coupling due to volume conduction[12,13].

To define coupling via coincident events, we applied oscillatory and aperiodic high-amplitude event detection using instantaneous frequency stability on source-reconstructed cortical activity over a broad range of frequencies (2–64 Hz; see Supplementary Text 1, Supplementary Fig. S1 and Methods). We validated this approach in three complementary ways. First, we showed that local high-amplitude oscillatory event-rates overlapped well with previously reported[46] cortical generators of oscillatory activity (see Supplementary Text 2 and Supplementary Fig. S2-S4). Second, we demonstrated that time-averaged networks of amplitude coupling components were reliable and, particularly, that networks defined by transient OECs predicted previously reported amplitude coupling features (See Supplementary Text 3 and Supplementary Fig. S5-S9). Third, we established that amplitude coupling network components were reliably and dynamically modulated during the task (Supplementary Text 4 and Supplementary Fig. S10-S13). We then moved on to relate the different coupling measures to different aspects of cognition during the task.

Coincidences of beta oscillatory events predict correct decisions

We found that OEC networks were dynamically modulated during our decision-making task[45] (Supplementary Text 4). We therefore asked whether the dynamics of transient amplitude co-fluctuation networks may predict decision behavior (Fig. 2). In a first step, we compared OEC dynamics between correct and error trials, matching the number of included (correct and error) trials by experimental conditions to discount effects of task difficulty and sensory salience (see Methods). Averaging over all significant connections ($n_{connection}$ = 104,196) and time points (4.5

seconds time window, n_{sample} = 1,800; paired t-test(19) between OECs in correct and error trials, $p<0.05$) we identified coupling increases during correct trials in the high alpha to beta frequency range (10–23 Hz) with a peak in the low-beta range at 16 Hz (Fig. 2a). We thus focused our initial analysis of performance related coupling on the beta range at 16 Hz. OEC rates increased particularly in the mid-decision phase around 1–2 seconds post-framing and right after stimulus offset (Fig. 2b). Correct choices were associated with coupling increases in a stable network of medial and lateral parietal, posterior temporal and lateral prefrontal areas (Fig. 2c), which appeared to be regulated over the decision phase without apparent network transitions (Fig. 2d). Furthermore, we identified a smaller subset of OEC connections that were relatively increased during error trials. We identified these connections predominantly in early visual and anterior temporal areas and mainly during the sensory and the early decision phase (Fig. 2b,c).

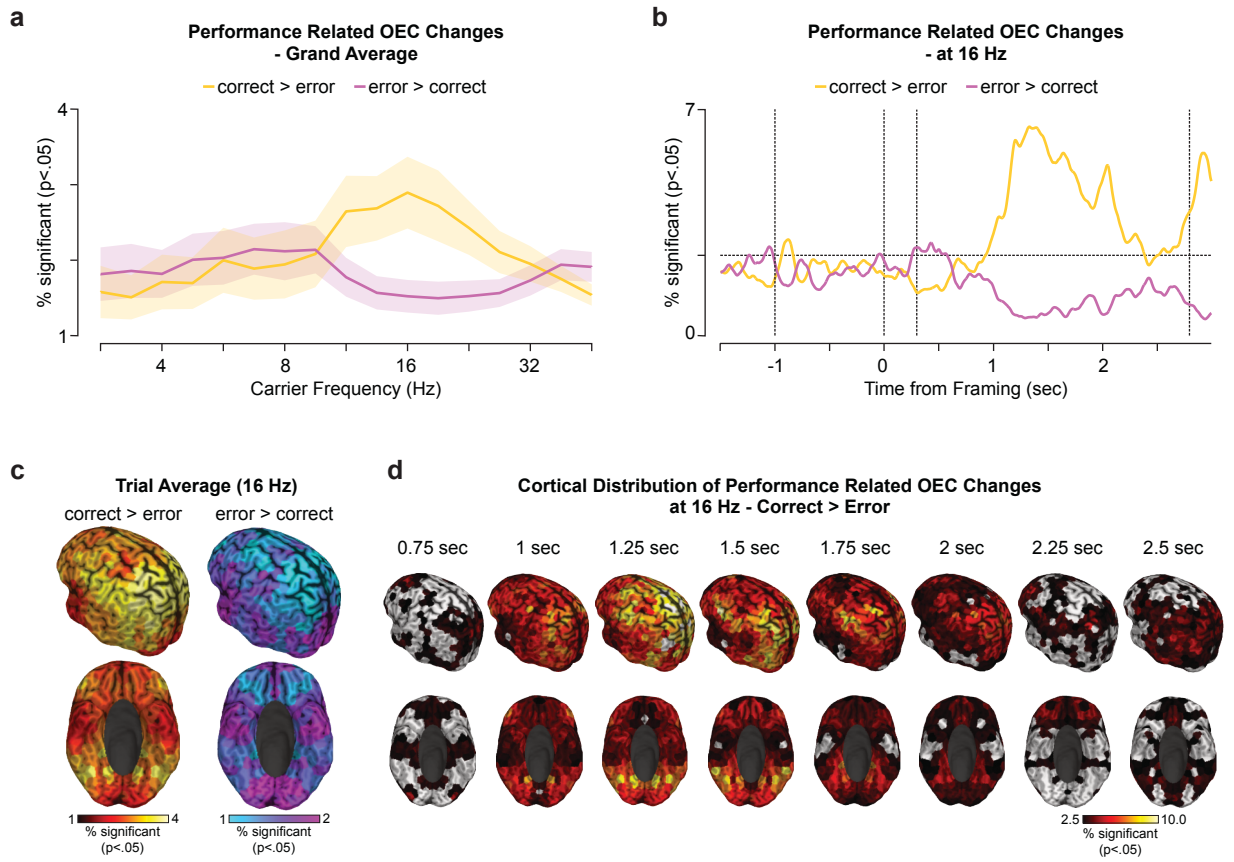

Figure 2 | Oscillatory event coincidence rate at 16 Hz increases prior to correct decisions. a Spectrum of the total number of performance related (correct vs. error, two-sided paired t-test(19), uncorrected p<.05) connections per cortical source averaged over the full trial length (-1.5–2.95 s with respect to the framing cue). Orange and purple lines indicate whether OEC was increased during correct and error trials, respectively. Lines and shaded areas indicate the mean and standard deviation over cortical sources. **b** Time course of the total number of performance related connections at 16 Hz (two-sided paired t-test(19), uncorrected p<.05; color coded as above). Vertical dashed lines denote the stimulus onset, framing cue on- and offset and the stimulus offset (from left to right). **c-d** Cortical distribution of the number of performance related connections per source averaged **c** over the full trial and **d** 0.5 s windows for correct > error (two-sided paired t-test(19), uncorrected p<.05). **d** Timing labels denote each window's starting time with respect to the framing cue onset. The color-scale displays the number of significantly increased (correct > error) OEC connections per time window. The results were averaged over hemispheres.

These findings show that transiently increased OECs can be predictive of behavior. Particularly, beta band coupling during the mid- and late stages of the trial increased during

correct but not error trials. An extended network of behaviorally relevant OECs hereby spanned the medial and lateral parietal as well as lateral prefrontal areas and the temporo-parietal junction. This beta OEC network appeared to be stable over time and was quantitatively up-/down-regulated throughout the decision phase.

Transient and sustained beta amplitude coupling networks dissociate in decision-making

Having demonstrated a relation of OECs in the beta range to behavior, we continued to quantify the behavioral relevance of OECs over the full spectrum. Further, we addressed the question whether partitioning amplitude coupling into transient (oscillatory and aperiodic) high-amplitude events and sustained (event free) activity can unravel distinct functional networks. Thus, we aimed at testing if any temporal, spectral or spatial features of decision-related network properties that can be attributed uniquely to transient OECs.

In the spectral domain we found widespread performance modulated OEC increases (correct > error) in the beta range (Fig. 3a) and less pronounced decreases (error > correct) peaking in the delta, alpha and gamma frequency ranges (Fig. 2a and Supplementary Fig. S14). Temporally, OEC increases occurred predominantly during the mid- and late decision phase (1–2.5 s from framing). On the other hand, OEC decreases peaked right after framing cue offset between 0.3 to 1 second post-framing. Spatially, the grand average of OEC network changes (Fig. 3b) overlapped strongly with the network identified at 16 Hz alone (Fig. 2). Yet, within each frequency we identified dissociable networks reflecting performance (Supplementary Fig. S15): Up to 8 Hz OECs increased in lateral parietal and lateral prefrontal areas. At 11 Hz we observed an extended parietal and posterior temporal network, while at 22 Hz OECs increased in medial parietal and lateral prefrontal areas. Performance-related OEC decreases were generally less pronounced (Supplementary Fig. S14 and S16).

Next, we compared these findings to performance related (correct versus error) amplitude coupling modulations with (Supplementary Fig. S15-S17) and without high-amplitude events (Fig.

3c,d). We found fewer and spectrally as well as spatially distinct performance related connections using sustained (event-free) amplitude coupling. Spectrally, sustained amplitude coupling decreased (error > correct) over the entire trial period in lower frequencies in the delta, theta and alpha range up to 8 Hz (Supplementary Fig. S14). Spatially, performance modulated increases (correct > error) occurred in a fronto-parietal and early visual network and decreases in a medial parietal, medial peri-central and ventral frontal network (Supplementary Fig. S15). Hereby, the cortical distribution of performance related sustained amplitude coupling appeared to be stable over frequencies yet most pronounced in the high alpha to beta range (8–23 Hz; Supplementary Fig. S15).

Transient aperiodic event coincidences showed performance related changes (correct > error) in a parietal, temporal and ventral stream visual network spatially overlapping with identified transient oscillatory network changes (compare Fig. 3b and Supplementary Fig. S18). However, transient aperiodic network changes were spectrally constrained to high frequencies in the high-beta to gamma range and to time points around stimulus offset.

Our results further indicated that amplitude coupling (including events) effects related to performance appeared to be a mixture of transient oscillatory network activity and sustained amplitude coupling (Supplementary Fig. S15-S17). We systematically correlated the behavioral effects, both in time and over the cortex. Interestingly, we found that OECs and event-free amplitude coupling showed little overlap below the gamma frequency range (Fig. 2e,f ; $R^2_{cortex,2.8\text{-}27Hz}$ = [<0.01, 0.54], $R^2_{time,2.8\text{-}27Hz}$ = [<0.01, 0.13]). Furthermore, amplitude coupling effects (including events) could to a large extent be explained through OECs for frequencies up to the beta ranges ($R^2_{cortex,2.8\text{-}23Hz}$ = [0.25, 0.71], $R^2_{time,2.8\text{-}23Hz}$ = [0.34, 0.95]). Yet, amplitude coupling (including events) overlapped with sustained low-amplitude coupling at higher frequencies (Supplementary Fig. S15e,f; $R^2_{cortex,27\text{-}45Hz}$ = [0.72, 0.97], $R^2_{time,27\text{-}45Hz}$ = [0.89, 0.99]).

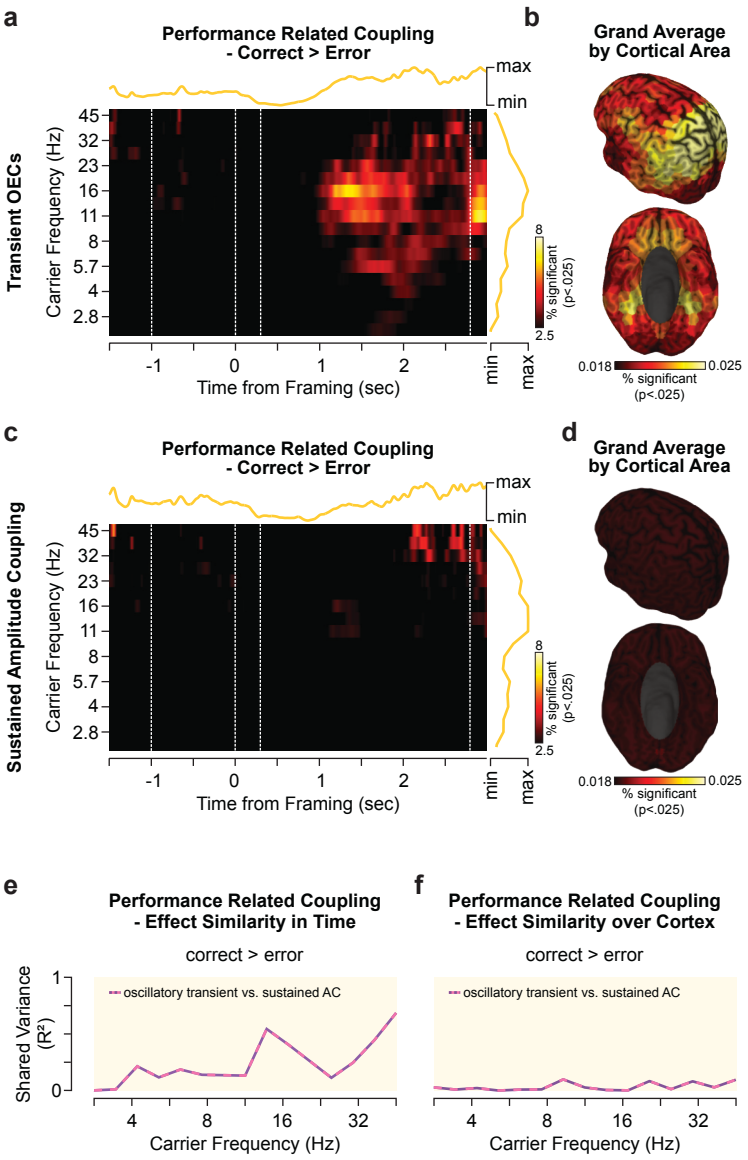

Figure 3 | Spectral and spatial dissociation of performance related amplitude coupling networks. a Time and frequency resolved distribution of performance related (correct > error, one-sided t-test(19), uncorrected p<.025) transient OEC connections. Colored lines on top and to the right denote the average over frequencies and time, respectively. **b** Average over the full time and frequency resolved distribution of performance related OEC modulations within each cortical source. **c-d** Same as **a-b** for sustained (event-free) amplitude coupling. **e-f** Pearson correlation of the behavioral coupling effects between transient oscillatory and sustained amplitude coupling (AC) comparing the **e** temporal (see Fig. 2a,c) and **f** spatial (Supplementary Fig. S15) distribution of effects. The values depict the shared variance (R^2) within each frequency.

All in all, transient high-amplitude oscillatory networks were modulated up to 1.5 seconds before a correct choice was made. OEC event rates increased particularly in the alpha and beta range (8–23 Hz) when participants made a correct choice. Our findings further demonstrate that decision-related functional networks dissociated temporally, spatially, spectrally and in magnitude between transient (events) and sustained (event-free) amplitude coupling modes. Importantly, our results show that the coincidence of transient high-amplitude oscillatory events might largely account for inter-areal interactions related to decision behavior.

Theta/alpha OECs orchestrate network dynamics during attention allocation

Our analyses described above show that transient and sustained components of dynamic amplitude coupling uncover distinct functional networks associated with behavioral performance in decision-making. We next studied the relation of these coupling patterns to another aspect of cognitive dynamics in our behavioral task: the spontaneous allocation of covert visual-spatial attention[47]. In a previous study[45] we showed that we can decode the momentary focus of attention and track brief covert allocations between decision alternatives[45,48], that can occur at any time during the trial. Covert attention strength intrinsically fluctuated around 9–12 Hz with attention reallocating between (switch) and refocusing on the same (stay) decision alternative at the trough and the peak of this oscillation, respectively[45].

Here, we asked if transient OECs and sustained amplitude coupling components were modulated differently during attention allocation. In a first step, we quantified attention-triggered OECs at 10 Hz separately around attention reallocation and refocus onset (Fig. 4a). When averaging over all connections we found a significant increase (two-sided, paired t-test(19), $p_{FDR}<0.05$) of OECs during attention reallocation compared to refocusing (switch vs. stay; see also Supplementary Fig. S19 for associated resting-state networks).

Next, we systematically assessed attention-related OEC rates over the entire spectrum and identified coupling modulations not only in the alpha but also the theta and beta frequency

ranges (Fig. 4b). On average over the cortex, between 9% (theta, 6 Hz) and 11% (alpha, 10 Hz) of all connections displayed increased transient OECs right around attention reallocation between alternatives (switch; per connection: paired t-test(19) of average OEC rate (-0.05–0.05 s from event), switch vs. stay, uncorrected $p<0.05$). Hereby, switch-related OECs were broadly increased, peaking in the theta and alpha frequency range (Supplementary Fig. S20-S22), in a network including ventral stream and early visual as well as medial parietal and lateral prefrontal areas (Fig. 4c). We identified fewer stay-related coupling changes (Fig. 4c and Supplementary Fig. S22). Transient aperiodic networks did not display a significant modulation with attention (Supplementary Fig. S23).

However, a very different relationship to cognition emerged for sustained amplitude coupling (Fig. 4d-f). While amplitude coupling including high-amplitude events mirrored our findings of attention-modulated OECs spectrally and spatially (Supplementary Fig. S21), we found marked differences when excluding all high-amplitude events. First, coupling within a lateral parietal and lateral prefrontal network was increased during reallocation (Fig. 4f) but we did not find an attention modulation of coupling within other attention networks or for the connection average (Fig. 4d and Supplementary Fig. S19b). Generally, over the entire spectrum fewer sustained amplitude coupling connections modulated with attention (Fig. 4e; compare to Fig. 4b; see also Supplementary Fig. S20-S22). Again, the smaller effect cannot be readily explained by weaker reliability (Supplementary Fig. S8) or statistical power. Further, we directly compared the attention-modulation effects between coupling components (Fig. 4g-i), i.e., correlation of frequency specific cortical distributions of attention modulation (see Supplementary Fig. S20 and S21). We found the highest correlation between OECs and amplitude coupling (including events; Fig. 4h) for frequencies below 32 Hz for attention reallocation networks (switch; $r_{switch,2.8\text{-}32Hz}$ = [0.62, 0.80]) and a high effect correlation between standard and sustained (event-free) amplitude coupling (Fig. 4i) at higher frequencies ($r_{switch,19\text{-}45Hz}$ = [0.62, 0.88]; $r_{stay,19\text{-}45Hz}$ = [0.50, 0.90]). Lastly,

OECs and sustained amplitude coupling effects displayed weaker correlations over the entire spectrum only exceeding |r| > 0.3 in the beta range ($r_{switch,16\text{-}27Hz}$ = [0.38, 0.65]; Fig. 4g).

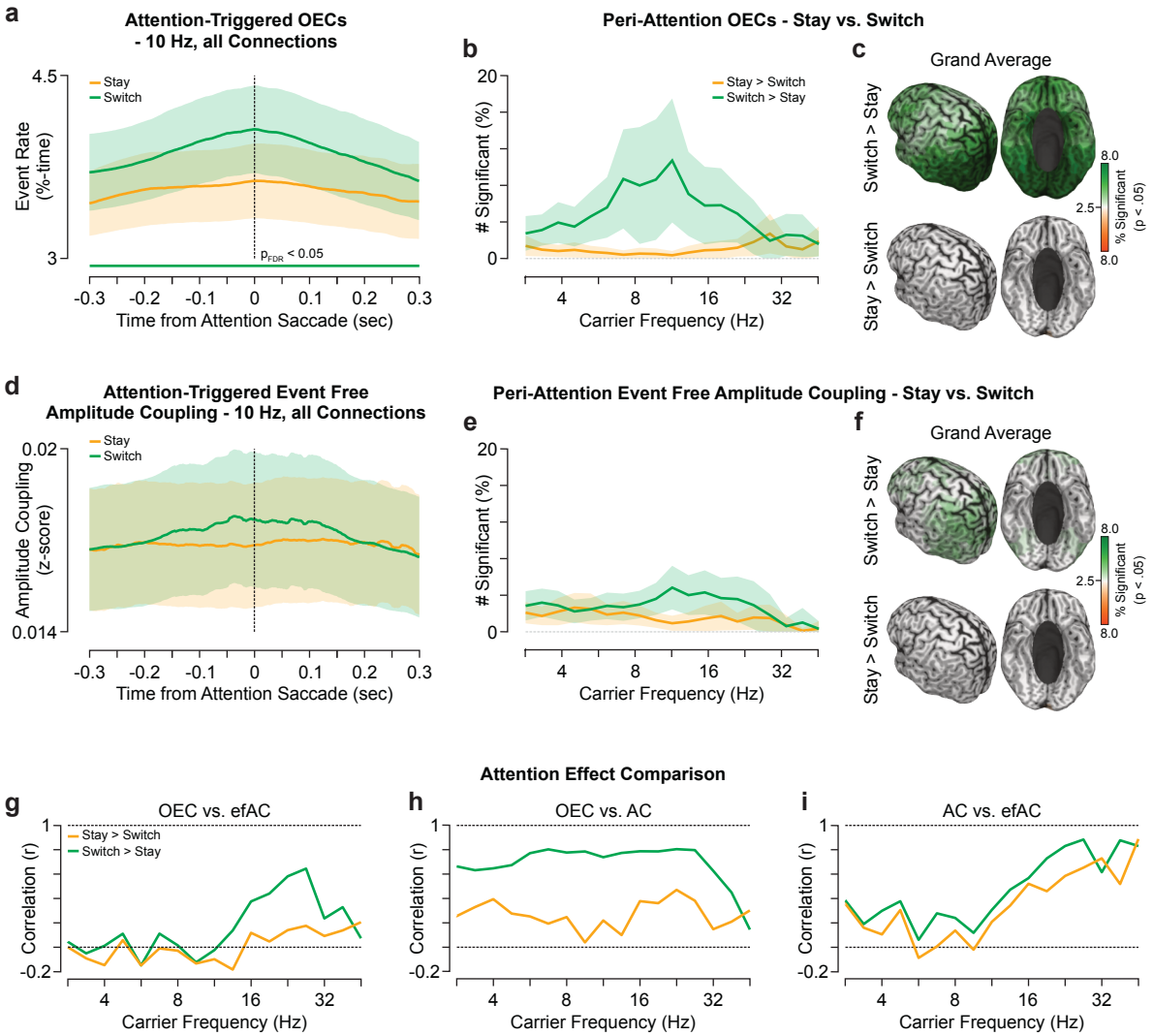

Figure 4 | Amplitude coupling components dissociate during attention reallocation. a Attention-triggered OECs at 10 Hz separately for attention reallocation (switch, green) and refocus (stay, orange) averaged over all connections. Colored lines and shaded areas denote the mean and standard deviation over participants (n = 20). Thick lines denote the time of significant difference between switch and stay (two-sided paired t-test(19), p_{FDR}<.05, FDR-corrected over time). **b** Number of OEC connections modulated by attention (paired two-sided t-test(19), uncorrected p<.05) at the time of attention allocation (averaged between -0.05 to 0.05 s) spectrally resolved between 2.8–45 Hz. Green and orange lines denote the mean proportion of connections per source increased during attention reallocation (switch) and

refocusing (stay), respectively. Shaded areas denote the standard deviation over cortical sources. **c** Grand average of the proportion of attention modulated OEC connections from each cortical source averaged over all frequencies. **d-f** The same as **a-c** for sustained (event-free) amplitude coupling. **g-i** Correlation of attention modulation effects between coupling measures. The correlations were computed between frequency-specific cortical distributions of the number of switch- and stay-modulated connections (see Supplementary Fig. S21 and S22) for **g** OEC against event-free amplitude coupling (efAC), **h** OEC against full amplitude coupling including events (AC), and **i** between efAC and AC. Color-coded as above.

Taken together, our results show that attention reallocation modulated transient oscillatory amplitude coupling. Transient OECs were enhanced in an extended visual, medial parietal and lateral prefrontal network predominantly in the theta and alpha frequency range at the moment of attention reallocation. The coupling effects for attention refocusing were generally weaker. After excluding high-amplitude events, sustained amplitude coupling displayed little attentional modulation. These findings further underline the functional, spatial and spectral dissociation between transient and sustained neuronal dynamics and their potentially distinct roles in large-scale cortical interactions during cognition.

Discussion

The exchange and integration of information over large distances in the brain is a prerequisite for flexible cognitive processing. Precise temporal relationships of neuronal activity reflected in phase coupling between distant areas have been associated with fostering and parsing this communication. However, little has been known about the functional role of correlated amplitude fluctuations of neural activity in long-distance communication and cognition. Leveraging the rich spatio-temporal resolution of non-invasive electrophysiological measurements we here demonstrate that short transients oscillatory dynamics are a central hallmark of large-scale neuronal interactions. We demonstrate that brief events of high-amplitude oscillatory activity govern the functional network dynamics during cognition. Our results show that coincidence of high-amplitude oscillatory events is relevant to decision behavior, indicative of better performance. Further, networks formed by the coincidence of oscillatory events coincidence were transiently modulated during attention allocation. Sustained low-amplitude co-fluctuations, on the other hand, showed a weaker modulation with cognition. Moreover, the networks defined by sustained and transient oscillatory coupling components were spatially and spectrally distinct. We, thus, conclude that not only sustained activity but particularly the orchestration of transient oscillatory events can facilitate inter-areal coupling and efficient cognition. Our results present initial evidence that different components of large-scale amplitude co-fluctuations might be associated with distinct neuronal circuit mechanisms.

Local activity strength and long-range co-fluctuations of signal amplitudes likely result from a mixture of several non-exclusive population-level mechanisms, including neuronal synchronization, firing rate modulations and neuromodulatory excitability fluctuations[1,3,8,43,44]. Neuronal synchronization reflects local excitability fluctuations temporally 'biasing' neuronal spiking, without necessitating changes in population firing rates, and resulting in (oscillatory) narrow-band frequency peaks of large-scale population signals[1,6,14,39,40]. Less rhythmic population

firing rate modulations can result in aperiodic spectral components in local field potentials[35,39–43,49]. Lastly, neuromodulatory systems can alter local excitability and the neuronal firing readiness[43]. The first two of these three mechanisms can further affect local population activity on very short time scales and might lead to the detection of high-amplitude events[3,32–34,36]. Here, we argue that large-scale oscillatory and aperiodic events, distinguished through signal rhythmicity[29,37], can serve as a potential handle for noninvasively studying the functional relevance of these population-level mechanisms: Large-scale aperiodic events might reflect scale-free firing rate modulations at the cellular level[3,42]. Similarly, the coincidence of high-amplitude oscillatory events between distant areas might display the orchestration of rhythmic excitability fluctuations between distant areas[3,6,7]. However, further research involving intracortical microscale recordings is needed to directly link oscillatory and aperiodic transients as well as sustained low-amplitude activity to neuronal and population level firing rate fluctuations and interactions.

Moreover, disentangling distinct components of large-scale amplitude coupling might enable the identification of distinct and temporally multiplexed channels for long-distance cortical information exchange. We found that sustained amplitude co-fluctuations as well as the co-occurrence of transient high-amplitude events, both oscillatory and aperiodic, demonstrated dissociable coupling and thus potentially distinct communication channels. Particularly brain-wide coupling of transient oscillatory events (i) demonstrated to be a reliable measure for functional networks, (ii) well explained previously reported amplitude coupling networks[12,13] while dissociating from sustained (event free) coupling from the delta up to the beta frequency range, and (iii) accorded for independent insights into cortical interactions during cognition. Overall, our results, thus, present amplitude co-fluctuations as an intrinsic coupling mode that might capture predominantly the orchestration between different transient oscillatory network states.

Disentangling different components of amplitude coupling can further help to directly test theories of large-cale neuronal communication. When local high-amplitude oscillatory events coincide across distant brain regions they also represent periods of heightened coherent

activity[3,8,9,30,31]. According to the 'Communication through Coherence' (CTC) model of large-scale interactions these periods are central to enabling/disabling direct information exchange by temporally aligning sender and receiver at an excitable or inhibitory phase, respectively[17,49]. Computational models have highlighted strong oscillatory activity as a prerequisite for CTC[9]. Thus, the inter-areal phase relationship during transient oscillatory events might be particularly relevant for effective communication: The phase relationship within each transient coincidence would define if information is processed and routed, i.e., during the excitable phase, or neglected, i.e., during the inhibitory phase, affecting behavior[8,16,47,49]. Our findings stipulate different predictions for two other concepts of large-scale communication: 'Coherence through Communication' (CTC*) and 'Communication through Resonance' (CTR)[3]. According to CTC*, coherence reflects statistical interactions between neuronal populations that occur through correlated output of the sending area with its own input to the receiving area. In contrast to CTC, here, the inter-areal phase-difference would be fixed via conduction delays and ion-channel time constants. Consequently, the phase relationship during coincident high-amplitude oscillatory events should be stable and independent of the cognitive state. In CTR, due to intrinsic structural properties of the receiving population, certain input frequencies elicit stronger responses leading to resonance with the sending population. Consequently, the instantaneous frequency of the sending units might show high variability, i.e., low rhythmicity, prior to establishing a transient interaction, indicating a transition towards the resonance frequency[3]. Overall, it appears pivotal to further assess the relationship of different amplitude coupling components and phase coupling to understand their roles in flexible information routing[3,8,20,35].

Another central finding of our study is that the coupling of transient and sustained signal components reveals spatially and spectrally dissociable networks that are known to be involved in distinct cognitive processes. First, during correct choices in our decision-making task sustained amplitude coupling occurred in the lateral parietal and medial prefrontal cortex; these areas are typically associated with integrative functions such as error monitoring and evidence

accumulation[50]. In contrast, transient oscillatory coupling increased between the medial, posterior parietal and lateral prefrontal areas, i.e., areas associated with output preparation and comparing sensory evidence[51]. Second, coincident oscillatory events were the coupling component that best represented brief attention reallocation, i.e., attentional saccades[48]. In the theta and high alpha frequency range a network of early visual, posterior parietal and lateral frontal areas was modulated during attention reallocation[45,48]. In contrast, keeping the focus of attention (refocus) was more strongly associated with sustained amplitude coupling in prefrontal areas. In sum, our findings provide preliminary evidence that cognitive processes involving either information integration or change detection might rely on communication channels utilizing either sustained or transient amplitude dynamics, respectively.

Our results contribute to the establishment of additional non-invasive markers for intrinsic large-scale interactions, which may aid the study of healthy and atypical neuronal communication in brain networks. Yet, there are limitations to the present results that can be addressed in future research. First, the potential relations between cognition, (oscillatory) signal strength dynamics and population-level mechanisms remain to be further elucidated. As we have pointed out above the link between the micro- and the macro-scale of neuronal activity needs to be investigated more directly. Second, pharmacological interventions might help to further address this relationship non-invasively. Critical dynamics, arousal and the balance between excitatory and inhibitory neural activity have been shown to influence oscillatory and aperiodic processes[37,39–41,43]. Pharmacological alterations of the excitation/inhibition ratio have quantifiable effects on local and inter-areal oscillatory and aperiodic activity in health[41,43]. Such pharmacological interventions could then also be leveraged to elucidate malfunctioning coupling in the diseased brain. Third, electrical stimulation can be applied noninvasively to identify causal links between neuronal coupling and cognition[7]. For example, amplitude-modulated transcranial alternating-current stimulation (AM-tACS) provides an approach to test effects of transient increases in oscillatory network activity. The principle of AM-tACS is to electrically stimulate neuronal tissue with a

sinusoidal carrier frequency that is modulated in strength over time. It can, thus, lead to entrainment of oscillatory processes that can display transiently enhanced activity at stimulation peaks[52].

In sum, our study show that amplitude coupling is a dynamically rich intrinsic coupling mode that is dominated by the coincidence of transiently high-amplitude oscillatory events. By identifying oscillatory event coincidences over the cortex we could reliably account for previously reported amplitude coupling networks in the delta, theta, alpha and beta frequency ranges with only a fraction of the data. Importantly, not every high-amplitude event is oscillatory, but transient increases of aperiodic activity might be another distinct feature of neuronal communication. Additionally, sustained amplitude coupling displayed reliable yet distinct network features. Averaging functional coupling over extended time periods might thus lump together various informative and dissociable processes. During cognitive processing sustained and transient coupling components might cater to qualitatively distinct functions and information processing time scales. Our results demonstrate that networks of coincident oscillatory events are a key signature of inter-areal interactions during cognition. We, thus, propose that efficient cognition and behavior may rely on information channels formed through co-occurring transient events.

Methods

Participants and experimental procedure

Participants. The task and participant group has been described in detail in[45]. In short, we tested twenty right-handed participants (9 female, age_{mean} = 28.05 years ± age_{STD} 4.6 years) in a decision-making task. The experiment was approved by the ethics committee of the Hamburg Medical Association and conducted in accordance with the Declaration of Helsinki. All participants gave their written informed consent and received monetary compensation for their participation.

Decision-making task. The main task was a three-alternative forced-choice protracted decision-making task with variable task framing. During central fixation three peripheral Gabor patches (2.2^o eccentricity, 1.6^o stimulus diameter) of varying contrast levels and orientations appeared simultaneously on screen (at the top and 120° left and right of it). The three stimuli were drawn from a set of five linearly spaced contrast levels (10 possible combinations, i.e., stimulus conditions). We used for each participant a staircase procedure to find the threshold physical distance between neighboring contrast levels and to control the task difficulty. The Gabor patch orientations were drawn from a set of three equally distant orientations with either all three being identical or different and pooled our analyses over orientation conditions. We did not utilize the orientation feature in the presented analyses.

Each trial started with the presentation of the central fixation cross. Participants were instructed to keep fixation and blink as little as possible during the trial. After 1 second the three Gabor patches appeared on screen and remained unaltered for 3.8 seconds. The task framing, i.e., if participants had to choose the highest ("Hig") or lowest ("Low") contrast, was centrally cued between 1–1.3 seconds into the stimulus presentation and randomized between trials. The high contrast stimulus represents the highest value in high framing trials, but the lowest value in low framing trials. The task framing divides the stimulus presentation period into the sensory- (pre-framing, -1–0 seconds from framing cue) and decision-phase (post-framing, 0.3–2.8 seconds)

with identical visual stimulation but distinct cognitive demands. After the 3.8 second stimulus presentation, the Gabor patches turned off and the response cue (fixation cross rotated 45°) started the maximum 2 seconds response window. Participants indicated their decision with a left thumb, right thumb or foot button press for the left, right or top alternative, respectively. We randomized the foot (left or right) between participants. We individually adjusted the height and location of the pedal for each participant using Styrofoam such that the position was comfortable and a response could be triggered with a small flexion of the porcellus fori. We gave binary feedback after each trial (fixation cross: green for correct, red incorrect). We fully randomized task framing, contrast levels, Gabor orientation and stimulus locations, yielding 1080 unique trials. Every participant concluded two full randomization runs. We blocked the trials into random 120-trial sets (n_{block} = 18). Participants chose the correct contrast on average in 77% of all trials (range = [66% 86%]). For the analyses comparing decision-making performance (correct vs. error) we matched the trials included for both performance levels by stimulus conditions and framing cue to account for difficulty and salience effects.

Stimulus localizer task. Prior to each block of the decision-making task the participants concluded a localizer block: 90 trials of consecutively presented single Gabor stimuli in one of the three locations at full contrast for 0.35 seconds with 0.5 seconds inter-trial intervals. The stimuli matched the decision-making task in size and eccentricity. Participants were instructed to ignore the peripheral stimuli, fixate at the center and detect a flickering of the central fixation cross that could occur randomly at each stimulus. In total, a flicker occurred 9 times per block, and participants indicated the detection with a button press. In each block we fully randomized the orientation and the position over the three locations. Each stimulus combination was repeated ten times paired once with a central fixation flickering. We used the localizer task to decode the visual representations of all three stimuli during the decision-making task.

Functional data acquisition and preprocessing

Data acquisition. During the experiment the participants were sitting upright in a whole-head magnetoencephalography scanner (MEG; 275 axial gradiometer sensors, CTF Systems Inc.) in a magnetically shielded room. The data was acquired at a sampling rate of 1200 Hz. Each participant's head position was tracked online using three head localization coils (nasion, left/right preauricular points). Additionally, we recorded a 2-channel bipolar electro-oculogram (horizontal and vertical EOG) and a single channel bipolar electro-cardiogram (ECG) to control for cardiovascular and ocular signal artifacts. Eye-movements and pupil diameter were tracked using an MEG-compatible Eyelink 1000 system (SR Research). We further collected T1-weighted structural magnetic resonance images (MRI; sagittal MP-RAGE) to reconstruct individualized high-resolution head models.

Preprocessing. The detailed MEG preprocessing pipeline can be found in[45]. We band-pass filtered the continuous MEG data segments between 0.2 and 200 Hz (4th order Butterworth filter) and down-sampled it to 400 Hz. We filtered the line noise with a notch filter at 50 Hz and its first 6 harmonics (1 Hz stop-band filter width). Next, we implemented a two-stage procedure for artifact rejection[53] applying filtering the signal into two distinct frequency ranges (low- from 0.2 to 30 Hz; high-range from 30 to 200 Hz), separately computed independent component analyses on each range and rejected artifact components based on their topology, power-spectra and time-courses[54].

Spectral analysis and source reconstruction

Spectral analysis. We generated time-frequency resolved MEG signals using Morlet's wavelets[53] (wavelet bandwidth at 0.5 octaves; $f/\sigma_f = 5.83$; kernel width covered $\pm 3\sigma_t$; σ_f and σ_t corresponds to standard deviation in frequency and time domain). We derived complex spectral estimates for frequencies between 2 to 90.5 Hz in quarter octave steps (2^1 to $2^{6.5}$ Hz).

Source projection. We generated single-shell boundary-element method models (BEM) based on individual structural MRIs. The physical forward model (leadfields) for 457 equally

spaced cortical sources (~1.2 cm distance, at 0.7 cm depth below pial surface) was computed using FieldTrip[55]. We applied dynamic imaging of coherent sources (DICS) linear beamforming to estimate the source-level neuronal activity. For seed-based analyses we used cortical source positions in the left auditory cortex (lAC, [-54, -22, 10]), left somatosensory cortex (lSSC, [-42, -26, 54]), medial prefrontal cortex (MPFC, [-3, 39, -2])[12], posterior medial temporal lobe (MT, [±39, -83, 15]), medial parietal cortex ([0, -64, 67]), lateral parietal cortex ([±41, -68, 44]), and lateral prefrontal cortex (PFC, [55, 13, 35]), all part of the source-model and in MNI-coordinates.

Defining transient high-amplitude events

We defined transient high-amplitude events as episodes of bandlimited high-amplitude activity. Here, we z-scored the squared amplitude, i.e., signal power, of the complex time-frequency resolved data over the full experiment within each cortical source. Prior to z-scoring, we subtracted the trial-averaged activity. Within each source and frequency, we recorded high-amplitude events as time points with a z-score larger 3.

Oscillatory vs. aperiodic events. To identify if a sample within a high-amplitude event is oscillatory or not, we leveraged the phase-progression stability of band-limited oscillatory activity[37]. A pure oscillation exhibits a progression through the phase cycle with uniform speed, i.e., a stable instantaneous frequency (see Supplementary Fig. S1). A filtered aperiodic signal on the other hand will display a more variable instantaneous frequency distribution through intrinsic frequency modulation. First, we computed for each time point $\boldsymbol{t}$ and source $\boldsymbol{i}$ the cross-spectrum c between the signal $\boldsymbol{x_t}$ with its past $\boldsymbol{x_{t-1}}$.

$$c_{i,t} = x_t * x'_{t-1}$$

Where $\boldsymbol{x'}$ denotes the complex conjugate of the signal. We then derived the first-order temporal derivative of the instantaneous phase $\Delta\varphi$ as the inverse tangent of the imaginary, divided by the real part of the cross-spectrum[29].

$$\Delta\varphi_{i,t} = \mathrm{atan}\left(\Im(c_{i,t})\,/\mathcal{R}(c_{i,t})\right)$$

The absolute value **||** of the instantaneous phase derivative describes the phase progression stability over time. The instantaneous frequency $\boldsymbol{f_{i,t}}$ can then be derived.

$$f_{i,t} = \left|\Delta\varphi_{i,t}\right|/(2 * pi) * f_{sample}$$

Where $\boldsymbol{f_{sample}}$ denotes the sampling frequency of the signal. Finally, we defined oscillatory time points as neighboring samples displaying the lowest first-order temporal derivative of the instantaneous frequency (IFD), i.e., moments of the most stable phase progression, by thresholding.

$$IFD = \left|\frac{df_i}{dt}\right| / f_{carrier}$$

$$IFD_{t,t+1} \begin{cases} < 0.0025 \in Osc \\ \geq 0.0025 \ \notin Osc \end{cases}$$

In other words, if the instantaneous frequency difference between neighboring samples, ***t*** and ***t+1***, is smaller than 0.25% of the carrier frequency $\boldsymbol{f_{carrier}}$ we considered time point ***t*** to be most likely oscillatory. For a pure sinusoid the IFD will be equal to zero (see Supplementary Fig. S1). Overall, the approach needs only three samples of the signal to generate a proxy of oscillatory activity, i.e., at a sampling rate of 400 Hz only 0.0075 seconds. The threshold parameter was derived as the approximate median 25th percentile of the IFD over the cortex at 11 Hz ($2^{3.5}$ Hz). Thus, at 11 Hz approximately 25% of time points for each source are set to be most likely oscillatory. We selected the alpha range as a reference frequency due to the large body of literature identifying oscillatory alpha activity[37,39,44]. We then applied the same threshold to all analyzed carrier frequencies. The threshold scales well with carrier frequency because the constructed Morlet wavelets filter widths are adaptive.

Lastly, we defined oscillatory and aperiodic high-amplitude events through the co-occurrence or not co-occurrence with a stable instantaneous frequency, respectively.

Analyzing event dynamics

Event rate and duration. We computed the local oscillatory event rate as the percentage of time points that an oscillatory event occurred at a given source and frequency. Under random conditions, i.e., no oscillatory activity, the minimum expected event rate can be derived from multiplying the probabilities of the signal crossing the amplitude and the IFD threshold (for frequencies: $median_{2\text{-}64Hz}$ = 0.26%, $range_{2\text{-}64Hz}$ = 0.03–0.34%). The relative event rate is the percentage of oscillatory events among all recorded high-amplitude events. Under random conditions the average relative oscillatory event rate would converge towards the probability of crossing the IFD threshold parameter (for frequencies: $median_{2\text{-}64Hz}$ = 29.3%, $range_{2\text{-}64Hz}$ = 2.7–35.2%). We applied fixed thresholds to explicitly address potential differences in the frequency-specific amplitude ($z_{threshold} > 3$) and instantaneous frequency ($\Delta f_{threshold} < 0.25\%$) distributions. The duration describes the median length of each high-amplitude event. Due to adaptive filter width of the applied Morlet wavelets the amplitude modulation can only depict a smaller range for lower frequencies and durations, measured in units of time, will be longer. We thus also computed the duration in units of cycle length by multiplying with the carrier frequency.

Functional coupling analyses

Amplitude coupling. We applied two different approaches to quantify the statistical relationships between the signal strength of distant cortical sources: amplitude coupling and event coincidences. For the amplitude coupling we pairwise multiplied (dot product) z-scored power envelope (squared amplitude) signals between a seed and a target region. These seed-target cofluctuations were either averaged over time, yielding the correlation coefficient (tima-averaged coupling analysis) or used to describe the temporal dynamics of amplitude coupling[29]. To discount effects of volume conduction, we orthogonalized the target- onto the seed signal prior to squaring and z-scoring the power envelopes[13]. The z-scoring was conducted over the full dataset within

each cortical source and frequency. For the full correlation matrices (source x source) we applied the orthogonalization in both direction with signals x and y as the seed and target and vice versa.

Coupling by event coincidence. We quantified coincidences of high-amplitude oscillatory events (OECs) between distant cortical sources as the "logical and" operation for the occurrence of high-amplitude events and stable instantaneous frequency in both the seed and target signals at the same time. Aperiodic events on the other hand showed high amplitude without IF stability in both sources. Hereby, the definition of high-amplitude events was based on the same orthogonalized z-scored power envelopes as the amplitude coupling. Coincidence under random conditions was estimated by multiplying the respective local event rates from seed and orthogonalized target, i.e., co-occurring events without temporal relationships between seed and target. The oscillatory (and aperiodic) coincidence time courses thus are binarized signals with zeros and ones indicating no coincidence and coincidence, respectively. Again, averaging these signals over time yields the coincidence rate for a specific connection (time-averaged coupling analysis), while the binary time courses were used to describe dynamic coupling with respect to external and internal events. Additionally, we computed event free amplitude coupling by excluding all local event time points from the seed-target power cofluctuations, i.e., we set high-amplitude event time points to nan (not a number).

Data simulation

To highlight the distinct features of oscillatory and aperiodic events we simulated 5 second traces of random data *x* with a pink noise spectrum (power ~ 1/f; $n_{simulation}$ = 100,000). We split each data trace into five 1-second windows (I-V). We multiplied the data in window II by 3 (*3x*) to increase broadband (aperiodic) power. We further multiplied window IV by 0.8 and added a constant 10 Hz sine wave *y* with an amplitude of 0.8 (*0.8x + 0.8y*), to increase oscillatory activity and bandlimited power. The modulation parameters were chosen to i) approximately match the broadband power between the random data segments (I, III, V) and the sine modulated window

IV as well as ii) approximately matching bandlimited power between 8–12 Hz for both modulated windows (II and IV). We estimated the broadband power within each window as the integral of the windowed Fourier transform. We applied the same Morlet wavelet transformation as outlined for the empirical data with a center frequency at 10 Hz and estimated the bandlimited power from the broadband Fourier transform solution between 8–12 Hz. We applied the event detection algorithm on the bandlimited full data trace while z-scoring the data according to the mean and standard deviation from windows I, III, and V for each simulation repetition. The IF stability threshold was set to the 10% percentile over windows I, III, and V.

Encoding the focus of covert attention

We used a stimulus localizer task to reconstruct the competition of stimulus representations during the decision-making task and thereby track the focus and strength of attention. Here, we implemented an inverted encoding model[45]. The encoding model assumes that the sum of abstract neuronal populations, i.e., information channels responsive to a given stimulus angle, is represented in the multivariate sensor-level MEG activity. Activity and tuning for an information channel can thus be estimated as the weighted sum of this MEG activity plus noise. The activity derived from inverting the model for MEG activity in the decision-making task then denotes momentary changes of the visual representations of the simultaneously presented stimuli.

Training the encoding model. We trained the encoding model on the retinotopic stimulus localizer task. During the localizer task only one stimulus out of the full set has been visible on screen. Hence, during the localizer both neuronal activity and the to be represented visual stimulus were known variables. We used bell-shaped tuning-curves (half-wave rectified sinusoidal) as design matrix to identify a linear weight-matrix relating neuronal activity and the presented stimuli[45]. We further used multivariate noise normalization on the weight-matrix to address correlated sensor activity, i.e., volume conduction, and improve reliability.

Applying inverted model on task data. With the optimized weight-matrix we can estimate the latent visual representation of the stimuli during the multi-alternative decision-making task. We inverted the model, i.e., the weight-matrix, and multiplied the MEG activity during the decision-making task. The solution of this operation yielded the representational activity over visual stimuli for each time point during the task. The strength of the representations is a proxy of covert visual attention towards each target on screen.

Reconstruction of attention focus. We used the vector sum of the three representational activities as a handle on the attention focus[45]. The vector orientations were set to 0°, 120° and 240° for the top, left and right stimulus, respectively and the representational activity corresponded to the length at each orientation. The reconstructed attentional vector can illustrate two features of visuo-spatial attention: First, the overall attention/alertness[56] paid to the stimuli and second, the main target of information sampling. Thus, we considered the length of the vector as a proxy for overall attention and the direction, i.e., the angular similarity to the three alternatives, as the most likely target of covert spatial attention at each time point. Importantly, this quantification of covert attention cannot be solely explained by fixational eye-movements or (micro-)saccades[45].

Model training parameter. We optimized the decoding performance within the localizer task by varying the training time point with respect to stimulus onset. Applying leave-one-block-out cross-validation (n_{block} = 18 per participant) we selected the time-window from 0.14–0.17 seconds after stimulus onset as training epoch[45]. For the model training we excluded stimulus localizer trials displaying (micro-)saccadic activity within the first 0.2 seconds after stimulus onset. On average 3% of all localizer trials per participant (mean = 3.03%, median = 1.82% range = 0.50% - 10.68%) were excluded.

Defining moments of attention reallocation and refocus. We leveraged the temporal dynamics of the attention vector to define moments when attention shifted from one alternative to another. The momentary focus of spatial attention was assessed via the angular similarity between the attention vector and the vector orientations corresponding to the three stimuli. At

every moment the vector can point close to one decision alternative or in between two options. We defined a threshold to identify time points where attention is focused at one alternative as the 90th percentile of the angular similarity distribution[45]. However, the vector is oriented in circular space and will even under random conditions, i.e., without visual stimulation or participant's alertness, point towards one of the three stimuli. We thus applied a second threshold on the vector length (within trial 90th percentile). An attentional saccade is only recorded when both thresholds, i.e., orientation and length of the vector, are crossed at the same time. We only recorded the first sample when both thresholds were crossed and excluded the following 0.025 seconds to not count individual events twice. We previously assessed the effects of different thresholds and concluded that the selected parameter range is sensible and does not qualitatively affect the conclusions on spatial attention (dynamics)[45]. Using this approach we identified 17,696 attention saccades per participant (median; range 12,377 to 28,909). We further tracked first-order sequences: Does an attention saccade focus on the same stimulus as the previous one ("stay", refocus) or shift between alternatives ("switch", reallocate). These sequences appear to be related to distinct attention functions and neuronal correlates[45].

Attention-related high-amplitude event dynamics. To assess the neuronal activity related to attention reallocation and refocus we computed the average event coincidence rate and amplitude coupling dynamics between 0.3 seconds before and after each attention reallocation/refocus. Importantly, we matched the included switch and stay by trial timing because the trial dynamics between both types vary[45]. Thus, we effectively included around 5,500 saccades per type and participant (median = 5,627, range = 3,824–10,771). We statistically tested neuronal activity between attention types, i.e., switch versus stay, applying paired t-tests of the attention-averaged activity for each sample within the attention-triggered time window (n_{sample} = 241). We applied false-discovery rate correction (FDR[57]) within each window. For analyses summarizing the activity directly at the events (for example Fig. 4) we first averaged the data between -0.05–0.05 seconds (relative to the event) before we conducted paired t-tests on the

time-averaged activity. For visualization we smoothed the peri-event activity by a 0.025s boxcar kernel.

Data and code availability

The processed data generated in this study will be made publicly available upon publication. The code for reproducing the main results and figures will be made publicly available upon publication.

Acknowledgements

This work was supported by grants from the European Research Council, project INFOSAMPLE, ERC-2018-StG-802905 (awarded to K.T.), and project cICMs, ERC-2022-AdG-101097402 (awarded to A.K.E.). Views and opinions expressed in this paper are those of the authors only and do not necessarily reflect those of the European Union or the European Research Council. Neither the European Union nor the granting authority can be held responsible for them. We thank Maryam Tohidi-Moghaddam for her help with the task design and data collection.

Author contributions

M.S., K.T. and Y.C. contributed to the experimental protocol. M.S. and Y.C. collected the data. M.S. conceptualized the functional coupling analysis. M.S. & Y.C. did the formal data analysis and M.S. visualized the results. M.S., T.H.D. & A.K.E. wrote the initial draft, all authors contributed to editing the manuscript. K.T. and A.K.E. acquired the funding for the study.

Declaration of competing interests

The authors declare no competing interests.

References

1. Buzsáki, G., and Draguhn, A. (2004). Neuronal Oscillations in Cortical Networks. Science *304*, 1926–1929. https://doi.org/10.1126/science.1099745.

2. Sabri, E., and Batista-Brito, R. (2025). Isolating single cycles of neural oscillations in population spiking. PLOS Comput. Biol. *21*, e1013084.

3. Vinck, M., Uran, C., Spyropoulos, G., Onorato, I., Broggini, A.C., Schneider, M., and Canales-Johnson, A. (2023). Principles of large-scale neural interactions. Neuron *111*, 987–1002.

4. Buzsáki, G., Anastassiou, C.A., and Koch, C. (2012). The origin of extracellular fields and currents—EEG, ECoG, LFP and spikes. Nat. Rev. Neurosci. *13*, 407–420.

5. Rosen, M.C., and Freedman, D.J. (2025). How distributed is the brain-wide network that is recruited for cognition? Nat. Rev. Neurosci., 1–13.

6. Engel, A.K., Gerloff, C., Hilgetag, C.C., and Nolte, G. (2013). Intrinsic coupling modes: multiscale interactions in ongoing brain activity. Neuron *80*, 867–886. https://doi.org/10.1016/j.neuron.2013.09.038.

7. Engel, A.K., and Gerloff, C. (2022). Dynamic functional connectivity: causative or epiphenomenal? Trends Cogn. Sci. *26*, 1020–1022.

8. Fries, P. (2015). Rhythms for Cognition: Communication through Coherence. Neuron *88*, 220–235. https://doi.org/10.1016/j.neuron.2015.09.034.

9. Akam, T.E., and Kullmann, D.M. (2012). Efficient "communication through coherence" requires oscillations structured to minimize interference between signals. PLoS Comput. Biol. *8*, e1002760. https://doi.org/10.1371/journal.pcbi.1002760.

10. Hayden, B.Y., Heilbronner, S.R., and Yoo, S.B.M. (2025). Rethinking the centrality of brain areas in understanding functional organization. Nat. Neurosci., 1–12.

11. Womelsdorf, T., Schoffelen, J.-M., Oostenveld, R., Singer, W., Desimone, R., Engel, A.K., and Fries, P. (2007). Modulation of Neuronal Interactions Through Neuronal Synchronization. Science *316*, 1609–1612. https://doi.org/10.1126/science.1139597.

12. Siems, M., and Siegel, M. (2020). Dissociated neuronal phase- and amplitude-coupling patterns in the human brain. NeuroImage, 116538. https://doi.org/10.1016/j.neuroimage.2020.116538.

13. Hipp, J.F., Hawellek, D.J., Corbetta, M., Siegel, M., and Engel, A.K. (2012). Large-scale cortical correlation structure of spontaneous oscillatory activity. Nat. Neurosci. *15*, 884–890. https://doi.org/10.1038/nn.3101.

14. Siegel, M., Donner, T.H., and Engel, A.K. (2012). Spectral fingerprints of large-scale neuronal interactions. Nat. Rev. Neurosci. *13*, 121–134. https://doi.org/10.1038/nrn3137.

15. Buschman, T.J., and Miller, E.K. (2007). Top-Down Versus Bottom-Up Control of Attention in the Prefrontal and Posterior Parietal Cortices. Science *315*, 1860–1862. https://doi.org/10.1126/science.1138071.

16. Rohenkohl, G., Bosman, C.A., and Fries, P. (2018). Gamma synchronization between V1 and V4 improves behavioral performance. Neuron *100*, 953–963.

17. Womelsdorf, T., and Fries, P. (2007). The role of neuronal synchronization in selective attention. Curr. Opin. Neurobiol. *17*, 154–160.

18. Fell, J., and Axmacher, N. (2011). The role of phase synchronization in memory processes. Nat. Rev. Neurosci. *12*, 105–118. https://doi.org/10.1038/nrn2979.

19. Buschman, T.J., Denovellis, E.L., Diogo, C., Bullock, D., and Miller, E.K. (2012). Synchronous Oscillatory Neural Ensembles for Rules in the Prefrontal Cortex. Neuron *76*, 838–846. https://doi.org/10.1016/j.neuron.2012.09.029.

20. Boroujeni, K.B., and Womelsdorf, T. (2023). Routing states transition during oscillatory bursts and attentional selection. Neuron *111*, 2929–2944.

21. Hipp, J.F., Engel, A.K., and Siegel, M. (2011). Oscillatory synchronization in large-scale cortical networks predicts perception. Neuron *69*, 387–396. https://doi.org/10.1016/j.neuron.2010.12.027.

22. Helfrich, R.F., Knepper, H., Nolte, G., Sengelmann, M., König, P., Schneider, T.R., and Engel, A.K. (2016). Spectral fingerprints of large-scale cortical dynamics during ambiguous motion perception. Hum. Brain Mapp. *37*, 4099–4111. https://doi.org/10.1002/hbm.23298.

23. Galindo-Leon, E.E., Hollensteiner, K.J., Pieper, F., Engler, G., Nolte, G., and Engel, A.K. (2025). Dynamic changes in large-scale functional connectivity prior to stimulation determine performance in a multisensory task. Front. Syst. Neurosci. *19*, 1524547.

24. Schölvinck, M.L., Leopold, D.A., Brookes, M.J., and Khader, P.H. (2013). The contribution of electrophysiology to functional connectivity mapping. Neuroimage *80*, 297–306.

25. Donner, T.H., Siegel, M., Fries, P., and Engel, A.K. (2009). Buildup of Choice-Predictive Activity in Human Motor Cortex during Perceptual Decision Making. Curr. Biol. *19*, 1581–1585. https://doi.org/10.1016/j.cub.2009.07.066.

26. Mostame, P., and Sadaghiani, S. (2020). Phase-and amplitude-coupling are tied by an intrinsic spatial organization but show divergent stimulus-related changes. NeuroImage, 219, Article 117051.

27. Galindo-Leon, E.E., Stitt, I., Pieper, F., Stieglitz, T., Engler, G., and Engel, A.K. (2019). Context-specific modulation of intrinsic coupling modes shapes multisensory processing. Sci. Adv. *5*, eaar7633.

28. Siems, M., Tünnerhoff, J., Ziemann, U., and Siegel, M. (2022). Multistage classification identifies altered cortical phase- and amplitude-coupling in Multiple Sclerosis. NeuroImage *264*, 119752. https://doi.org/10.1016/j.neuroimage.2022.119752.

29. Tewarie, P., Liuzzi, L., O'Neill, G.C., Quinn, A.J., Griffa, A., Woolrich, M.W., Stam, C.J., Hillebrand, A., and Brookes, M.J. (2019). Tracking dynamic brain networks using high temporal resolution MEG measures of functional connectivity. NeuroImage *200*, 38–50.

30. Hindriks, R., and Tewarie, P.K. (2023). Dissociation between phase and power correlation networks in the human brain is driven by co-occurrent bursts. Commun. Biol. *6*, 286.

31. Seedat, Z.A., Quinn, A.J., Vidaurre, D., Liuzzi, L., Gascoyne, L.E., Hunt, B.A.E., O'Neill, G.C., Pakenham, D.O., Mullinger, K.J., Morris, P.G., et al. (2020). The role of transient spectral 'bursts' in functional connectivity: A magnetoencephalography study. NeuroImage *209*, 116537. https://doi.org/10.1016/j.neuroimage.2020.116537.

32. Lundqvist, M., Miller, E.K., Nordmark, J., Liljefors, J., and Herman, P. (2024). Beta: bursts of cognition. Trends Cogn. Sci.

33. Tal, I., Neymotin, S., Bickel, S., Lakatos, P., and Schroeder, C.E. (2020). Oscillatory bursting as a mechanism for temporal coupling and information coding. Front. Comput. Neurosci. *14*, 82.

34. van Ede, F., Quinn, A.J., Woolrich, M.W., and Nobre, A.C. (2018). Neural oscillations: sustained rhythms or transient burst-events? Trends Neurosci. *41*, 415–417.

35. Banaie Boroujeni, K., Helfrich, R.F., Fiebelkorn, I.C., Bentley, J.N., Brunner, P., Lin, J.J., Knight, R.T., and Kastner, S. (2025). High-frequency bursts facilitate fast communication for human spatial attention. Nat. Neurosci., 1–10.

36. Kosciessa, J.Q., Grandy, T.H., Garrett, D.D., and Werkle-Bergner, M. (2020). Single-trial characterization of neural rhythms: Potential and challenges. NeuroImage *206*, 116331.

37. Myrov, V., Siebenhühner, F., Juvonen, J.J., Arnulfo, G., Palva, S., and Palva, J.M. (2024). Rhythmicity of neuronal oscillations delineates their cortical and spectral architecture. Commun. Biol. *7*, 405.

38. Schmidt, R., Rose, J., and Muralidharan, V. (2023). Transient oscillations as computations for cognition: Analysis, modeling and function. Curr. Opin. Neurobiol. *83*, 102796.

39. Donoghue, T., Haller, M., Peterson, E.J., Varma, P., Sebastian, P., Gao, R., Noto, T., Lara, A.H., Wallis, J.D., and Knight, R.T. (2020). Parameterizing neural power spectra into periodic and aperiodic components. Nat. Neurosci. *23*, 1655–1665.

40. Voytek, B., and Knight, R.T. (2015). Dynamic network communication as a unifying neural basis for cognition, development, aging, and disease. Biol. Psychiatry *77*, 1089–1097. https://doi.org/10.1016/j.biopsych.2015.04.016.

41. Arazi, A., Toso, A., Grent-‘t-Jong, T., Uhlhaas, P.J., and Donner, T.H. (2025). Large-scale maps of altered cortical dynamics in early-stage psychosis are related to GABAergic and glutamatergic neurotransmission. Sci. Adv. *11*, eads0400.

42. Vinck, M., Uran, C., Dowdall, J.R., Rummell, B., and Canales-Johnson, A. (2024). Large-scale interactions in predictive processing: oscillatory versus transient dynamics. Trends Cogn. Sci.

43. Pfeffer, T., Ponce-Alvarez, A., Tsetsos, K., Meindertsma, T., Gahnström, C.J., van den Brink, R.L., Nolte, G., Engel, A.K., Deco, G., and Donner, T.H. (2021). Circuit mechanisms for the chemical modulation of cortex-wide network interactions and behavioral variability. Sci. Adv. *7*, eabf5620.

44. Ibarra Chaoul, A., and Siegel, M. (2021). Cortical correlation structure of aperiodic neuronal population activity. NeuroImage *245*, 118672. https://doi.org/10.1016/j.neuroimage.2021.118672.

45. Siems, M., Cao, Y., Tohidi-Moghaddam, M., Donner, T.H., and Tsetsos, K. (2025). Rhythmic sampling of multiple decision alternatives in the human brain. bioRxiv, 2023.12.08.570734. https://doi.org/10.1101/2023.12.08.570734.

46. Capilla, A., Arana, L., García-Huéscar, M., Melcón, M., Gross, J., and Campo, P. (2022). The natural frequencies of the resting human brain: An MEG-based atlas. NeuroImage *258*, 119373.

47. Fiebelkorn, I.C., and Kastner, S. (2020). Functional specialization in the attention network. Annu. Rev. Psychol. *71*, 221–249.

48. Gaillard, C., Ben Hadj Hassen, S., Di Bello, F., Bihan-Poudec, Y., VanRullen, R., and Ben Hamed, S. (2020). Prefrontal attentional saccades explore space rhythmically. Nat. Commun. *11*, 925. https://doi.org/10.1038/s41467-020-14649-7.

49. Fries, P. (2023). Rhythmic attentional scanning. Neuron *111*, 954–970. https://doi.org/10.1016/j.neuron.2023.02.015.

50. Okazawa, G., and Kiani, R. (2023). Neural mechanisms that make perceptual decisions flexible. Annu. Rev. Physiol. *85*, 191–215.

51. Heekeren, H.R., Marrett, S., and Ungerleider, L.G. (2008). The neural systems that mediate human perceptual decision making. Nat. Rev. Neurosci. *9*, 467–479.

52. Wu, L., Liu, T., and Wang, J. (2021). Improving the effect of transcranial alternating current stimulation (tACS): A systematic review. Front. Hum. Neurosci. *15*, 652393.

53. Siems, M., Pape, A.-A., Hipp, J.F., and Siegel, M. (2016). Measuring the cortical correlation structure of spontaneous oscillatory activity with EEG and MEG. NeuroImage *129*, 345–355. https://doi.org/10.1016/j.neuroimage.2016.01.055.

54. Hipp, J.F., and Siegel, M. (2013). Dissociating neuronal gamma-band activity from cranial and ocular muscle activity in EEG. Front. Hum. Neurosci. *7*, 338. https://doi.org/10.3389/fnhum.2013.00338.

55. Oostenveld, R., Fries, P., Maris, E., and Schoffelen, J.-M. (2011). FieldTrip: open source software for advanced analysis of MEG, EEG, and invasive electrophysiological data. Comput. Intell. Neurosci. *2011*, 156869.

56. Cook, A.J., Im, H.Y., and Giaschi, D.E. (2025). Large-scale functional networks underlying visual attention. Neurosci. Biobehav. Rev. *173*, 106165. https://doi.org/10.1016/j.neubiorev.2025.106165.

57. Benjamini, Y., and Hochberg, Y. (1995). Controlling the False Discovery Rate: A Practical and Powerful Approach to Multiple Testing. J. R. Stat. Soc. Ser. B Methodol. *57*, 289–300.